Numerical modelling and simulation of membrane-based extraction of copper(II) using hollow fiber contactors

Amir Muhammad, Mohammad Younas, Stéphanie Druon-Bocquet, Julio Romero, José Sanchez-Marcano

Numerical modelling and simulation of membrane-based extraction of copper (II) using hollow fiber contactors

Article *in* Desalination and Water Treatment · December 2016

DOI: 10.5004/dwt.2017.20169

CITATIONS
5

READS
156

4 authors, including:

Julio Romero
University of Santiago, Chile
117 PUBLICATIONS **1,995** CITATIONS
SEE PROFILE

José Sanchez Marcano
European Institute of Membranes
228 PUBLICATIONS **3,862** CITATIONS
SEE PROFILE

Desalination and Water Treatment
www.deswater.com

doi: 10.5004/dwt.2017.20169

63 (2017) 113–123
February

Numerical modelling and simulation of membrane-based extraction of copper (II) using hollow fiber contactors

Amir Muhammad[a], Mohammad Younas[a,*], Stéphanie Druon-Bocquet[b], Julio Romero[c], José Sanchez-Marcano[b]

[a]*Department of Chemical Engineering, University of Engineering and Technology, Peshawar, P.O. Box 814, University Campus, Peshawar 25120, Pakistan, Tel. +92919218180; emails: m.younas@uetpeshawar.edu.pk (M. Younas), engr.amir@uetpeshawar.edu.pk (A. Muhammad)*
[b]*Institut Européen des Membranes, UMR 5635, CNRS, ENSCM, UMII, Université de Montpellier II, CC 047, 2 Place Eugène Bataillon, 34095 Montpellier cedex 5, France, Tel. +33 4 67 14 91 65; email: Stephanie.Druon-Bocquet@univ-montp2.fr (S. Druon-Bocquet), Tel. +33 4 67 14 91 49; email: Jose.Sanchez-Marcano@univ-montp2.fr (J. Sanchez-Marcano)*
[c]*Laboratory of Membrane Separation Processes (LabProSeM) Department of Chemical Engineering, University of Santiago de Chile, Av. Lib. Bdo. O'Higgins 3363, Estación Central, Santiago, Chile, Tel. +56 2 718 18 21; email: julio.romero@usach.cl*

Received 20 May 2016; Accepted 14 August 2016

ABSTRACT

This work describes the mathematical modelling and numerical simulation of a hollow fiber membrane contactor for copper (II) extraction from aqueous solutions with 1,1,1-trifluoro-2,4-pentanedione commonly known as TFA diluted in n-decanol. Model was developed for convection–diffusion mass and momentum transfer using continuity and Navier–Stokes equations. Model equations were solved using a computational fluid dynamics code, and results were validated with experimental data. After validation of model, simulation was performed to check the effects of hydrodynamics conditions on contactor performance. 49% of copper (II) was extracted from aqueous solution for feed flow rate of 8.3×10^{-7} $m^3.s^{-1}$, and for partition coefficient equals to 1. However, simulation results indicated that extraction could be greatly improved by decreasing feed flow and increasing partition coefficient. Simulation was also run to study the distribution profiles of copper (II) concentration, flux and velocity in 2-D.

Keywords: Copper (II); Dispersion free extraction; Hollow fiber membrane contactor; Computational fluid dynamics; TFA

1. Introduction

Copper (II) recovery from aqueous streams has always been a relevant research area due to its importance from environmental perspective or in the context of hydrometallurgical process [1–3]. Membrane-based solvent extraction representing a non-dispersive phase contact operation, in which the interface between feed and extractant streams is supported by a macroporous membrane wall, is a useful emerging technique for copper (II) extraction. In this process, mixing of phases is avoided, and problems of flooding, entraining or downstream phase separation do not occur [4]. Moreover, on the contrary to classical extraction columns, there is no need for density differences between the feed and extractant, leading to a greater choice of extractants. Hollow fiber membrane contactors (HFMCs) offer several advantages such as: compact process design, modularity, controlled interfacial area and higher volumetric efficiency due to large specific contact area [5–7].

Extensive research work has been reported on extraction processes based on HFMCs by several research teams like Prasad and Sirkar [8], Yang and Cussler [9] as well as extensive review by Gabelman and Hwang [10] and Pabby and

* Corresponding author.

Sastre [11]. HFMCs have been used in extraction processes for the last 2 decades [12]. Extraction of copper (II) using chelating extractants like LIX 84-1 and LIX 622N has been widely studied [13–15]. Literature study reviewed that experimental investigation covered the extraction kinetics, distribution equilibria and dispersion-free extraction of copper (II) with extractants. Nonetheless, not enough literature on theoretical study of copper (II) with extractants using HFMC is available. Furthermore, 1,1,1-trifluoro-2,4-pentanedione (TFA) has not been used as extractant for copper (II) extraction, although TFA has been found to be an efficient extractant for copper (II) extraction [16,17].

Mass transfer in membrane contactors has been modelled by several research teams with resistance-in-series approach [10,12,18,19]. This approach is based on three mass transfer resistances in series as solute moves from feed to solvent across membrane. Models developed with this approach were analytically solved and based on negligible axial diffusion. Mass transfer coefficients were estimated from empirical correlations, which are not very accurate. Meanwhile, numerical models and their solutions offer a description of axial diffusion approximation. These models are based on mass and momentum balance equations and do not require estimation of mass transfer coefficients. Numerical analysis and simulation also known as computational fluid dynamics (CFD) of HFMC offer a detailed description of solute transfer across the membrane surface [20–23]. In recent years, several researchers used CFD to describe mass and momentum transport through HFMC [24–26]. Although comprehensive 2-D model was developed and simulated for gas absorption [27–30], simulation of mass and momentum transport of liquid–liquid extraction, in general, and of copper (II) extraction, in particular, through HFMC is lacking in literature. Marjani and Shirazian [31], Rezakazemi et al. [32] and Nosratinia et al. [33] studied the numerical simulation of ammonia removal from wastewaters using membrane contactors. Ghadiri and Shirazian [34] investigated computational simulation of mass transfer in extraction of alkali metals through membrane contactors. Fadaei et al. [35] simulated the membrane contactor for copper (II) extraction with di-(2-ethylhexyl)phosphoric acid (D2EHPA) through CFD techniques. Effect of partition coefficient and profile study of hydrodynamics have not yet been studied for membrane-based solvent extraction of copper (II).

This work proposes a steady-state numerical model of an HFMC to study the behavior of copper (II) extraction from an aqueous phase using an organic phase containing TFA as extractant agent. The objective of the current work is the identification and description of the copper (II) transfer mechanism in liquid–liquid HFMC through CFD. Numerical model was developed on a hypothesized symmetrical unit of HFMC. Concentration profile for copper (II) extraction with TFA through convective and diffusive mass transport in a hollow fiber contactor was developed. The model was then integrated in a more global model taking also into account feed and solvent phase recycling. The integrated model of the extraction process was validated with experimental results. Simulations were done in order to assess the effect of the operating variables on the concentration and flux profiles of copper (II) as well as on the velocity profiles in the contactor. Partition coefficient and fluid flow rates effects upon extraction efficiency were also investigated.

2. Materials and methods

2.1. Reagents and solutions

1-Decanol and TFA were obtained from Sigma-Aldrich® (France) and used without further purification. Their characteristics such as density and viscosity were found in Rigglo et al. [36], Faria et al. [37] and Mutalik et al. [38] or provided by the manufacturer. The feed solution is an aqueous solution of copper (II) prepared by dissolving analytical reagent grade $CuSO_4.5H_2O$ (purchased from Fisher Chemical®, France) in deionized water. A master solution of 15.75 mol m^{-3} of copper (II) was prepared and was then diluted to 7.87 and 3.15 mol m^{-3} or less as per requirement. Organic phase was prepared by dissolving the known volume of TFA in the desired diluent.

2.2. Membrane process configuration and its properties

The experimental work was based on dispersion-free extraction of copper (II) from the feed with TFA through the HFMC. The hollow fiber contactor module was provided by Liqui-cel™ (USA). Copper (II) solution was prepared by dissolving $CuSO_4$ in deionized water to achieve the desired copper (II) concentration. TFA was used as extractant agent and was diluted in n-decanol. The runs were carried out at room temperature (298 ± 5 K). The schematic setup of the plant is shown in Fig. 1. The aqueous and organic phase volumes were taken as 1.0×10^{-3} m^3 in two storage tanks and were agitated constantly by magnetic stirrers.

Aqueous feed stream with known copper (II) concentration (3.15 mol m^{-3}) was fed inside the fibers. Organic phase was flown countercurrently in the shell side. The concentration of TFA was taken as 160 mol.m^{-3}. This achieves the partition coefficient value of 1 [16,17]. As the membrane material was hydrophobic, the organic phase penetrated through the pores of the membrane and immobilized up to the pores mouth at the aqueous phase-membrane interface. A pressure of 180 kPa was exerted on aqueous phase side of the fiber preventing the organic phase flow to enter into the lumen side. Nonetheless, the exerted pressure was less than the critical penetration pressure in order to prevent the mixing of both phases [39]. Aqueous phase samples,

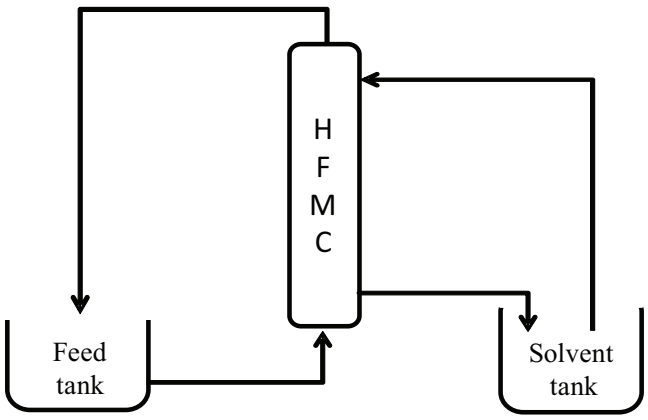

Fig. 1. Experimental set up: recycled copper (II) extraction with TFA in HFMC.

Table 1
Geometrical and simulation parameters of the hollow fiber membrane contactor module (X-50) considered for simulations [16,40]

Parameters	Symbols	Values
Fiber inside radius	R_1	1.1×10^{-4} m
Fiber outside radius	R_2	1.5×10^{-4} m
Flow-cell (shell side) radius	R_3	2.47×10^{-4} m
Length of the module	L	121.8×10^{-3} m
Porosity	ε	0.4
Tortuosity	τ	1/ε
Packing fraction	P_f	0.37
Number of fibers	n	7,400
Diffusion coefficient of Cu(II) in aqueous side (tube side)	D_{aq}	2.79×10^{-9} m^2.s^{-1}
Diffusion coefficient of Cu-TFA complex in organic side (shell side)	D_{org}	1.23×10^{-10} m^2.s^{-1}
Diffusion coefficient of Cu-TFA complex compound in membrane	D_{mem}	D_{org} (ε/τ) m^2.s^{-1}
Initial concentration of copper (II) in aqueous phase	C_{ini}	3.15 mol.m^{-3}
Initial concentration of TFA in organic phase	C_{org}	160 mol.m^{-3}
Partition coefficient	P	1
Velocity of aqueous phase	V_{aq}	0.0033 m.s^{-1}
Velocity of organic phase	V_{org}	0.0017 m.s^{-1}

at different pre-assumed time intervals, were taken from aqueous phase storage tank during the experiment, and the concentration of copper (II) was quantified by atomic absorption spectrometry. Prior to experiments, deionized water and organic phase solution were introduced into the membrane module for at least 30 min or till the stabilization of operating parameters like temperature, flow rates and pressure drop. Time delays could also occur in achieving steady state; however, these effects were neglected in model formulation. The deionized water phase was then replaced with an aqueous phase solution containing copper (II). Experiments lasted for about 70–90 min. Physicochemical and transport properties of both phases and geometrical parameters of the membrane contactor are summarized in Table 1.

3. Theoretical description of the mass transfer

3.1. Model approach and its considerations

Fibers of the contactor were assumed as regularly packed axially in the shell of the HFMC module. Each fiber had its hypothesized flow area. This original configuration, named as "flow-cell", resembled a concentric circular tube where the thickness of the inner tube denoted the thickness of the porous membrane [40]. The module was an assembly of identical "flow-cells" parallel to each other. The model behavior of single "flow-cell" was extrapolated to the whole contactor. Three sections of a single "flow-cell", i.e., tube side, membrane and shell side are shown schematically in Fig. 2. The model domain and its boundaries are also shown. R_1, R_2 and R_3 denote the inner radius of fiber, outer radius of fiber and the "flow-cell" radius, respectively. The radial position of a single "flow-cell" section, R = 0, shows the center of fiber. C_1, C_2 and C_3 are concentrations of copper (II) in aqueous phase, membrane pores and organic phase, respectively. These concentrations depend on axial (z) and radial (r) positions of the module.

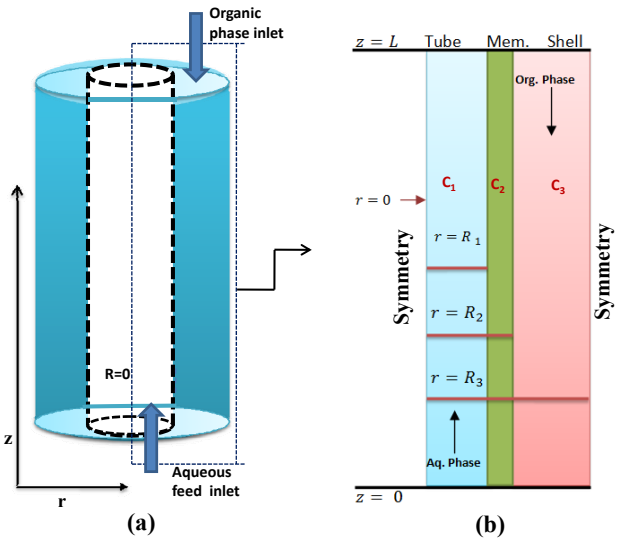

Fig. 2. (a) Hypothetical single fiber flow-cell HFMC module and (b) single axial–radial flow-cell with model domain and its boundaries.

Copper (II) is considered as complexed with TFA at the interface, and this process was considered fast enough to achieve equilibrium at the interface on aqueous phase boundary layer [16,17]. TFA–Cu^{2+} complex formation at interface could be taken as a hypothetical simple extraction. Apparent partition coefficient between both phases: copper (II) in aqueous phase and TFA–Cu^{2+} in organic phase was considered in model development.

The description of copper (II) transfer involved the development of a mathematical model based on mass and momentum conservation equations, which have been applied in three sections at proximities of the membrane contactor. Following assumptions have been made while deriving mass and momentum conservation equations:

- Both liquids were assumed to be incompressible and Newtonian fluids.
- Steady-state conditions were considered.
- The membrane was exclusively wetted by organic phase.
- No mixing of aqueous and organic phases.
- No convective mass transfer through membrane's pores.
- Flow was laminar in both sides of the contactor.
- The flow in lumen side was fully developed.
- Equilibrium was established at interface of aqueous phase boundary layer.
- The system was isothermal.
- Partition coefficient was assumed to remain constant throughout contactor.

3.2. Governing equations

Transport of copper (II) in fibers of the module occurs due to convection–diffusion mass transfer. The transfer of copper (II) with chemical reaction and for unsteady-state conditions could be described by the following continuity equation [41]:

$$\frac{\partial C_{i,aq}^{'}}{\partial t} = -\nabla.N_i + R_i^{'} \tag{1}$$

where $C_i^{'}$ is the dimensionless concentration given as:

$$C_i^{'} = C_i / C_0$$

C_i is the concentration of solute at any point in membrane module, while C_0 is the inlet concentration.

In Eq. (1), N_i is the combined flux (diffusive + convective); $R_i^{'}$ denotes the reaction rate of the specie *i* and subscript "*aq*" is written for aqueous phase.

∇ is gradient vector given as:

$$\nabla = \frac{\partial}{\partial R} \text{ or } \frac{\partial}{\partial Z}$$

where *R* and *Z* are given as follows:

$$R = r/R_3,\ Z = z/L$$

where *r* and *z* are radial and axial axis, respectively, while *L* denotes total length of module.

According to Fick's law, combined flux could be estimated by:

$$N_i = -D_{i,aq}\nabla C_{i,aq}^{'} + C_{i,aq}^{'}u_{z,aq} \tag{2}$$

where $D_{i,aq}$ is the diffusion coefficient of specie *i* in aqueous phase, and $u_{z,aq}$ is axial velocity of aqueous phase along the length of module. The two terms on right-hand side of Eq. (2) show diffusive and convective fluxes, respectively.

Combining Eqs. (1) and (2) results in Eq. (3):

$$\frac{\partial C_{i,aq}^{'}}{\partial t} = D_{i,aq}\nabla C_{i,aq}^{'} - C_{i,aq}^{'}u_{z,aq} + R_i^{'} \tag{3}$$

As mentioned earlier, the reaction between solute and organic extractant could be considered as instantaneous at aqueous phase interface, and the term $R_i^{'}$ in Eq. (3) vanishes. Thus, it can be described by the partition coefficient at the interface of aqueous phase boundary layer with the membrane. At steady-state condition, accumulation term becomes null, so Eq. (3) takes the following form in cylindrical coordinates:

$$D_{i,aq}\left[\frac{\partial^2 C_{i,aq}^{'}}{\partial R^2} + \frac{1}{r}\frac{\partial C_{i,aq}^{'}}{\partial R} + \frac{\partial^2 C_{i,aq}^{'}}{\partial Z^2}\right] = u_{Z,aq}\frac{\partial C_{i,aq}^{'}}{\partial Z} \tag{4}$$

As the flow inside the fiber was assumed to be laminar and fully developed, the velocity distribution of aqueous phase could be given by [41]:

$$u_{z,aq} = 2u\left[1 - \left(\frac{r}{R_1}\right)^2\right] \tag{5}$$

where *u* is the mean velocity of aqueous phase inside the fiber.

Transfer of solute across the hydrophobic membrane occurs through diffusion and is given by following steady-state continuity equation:

$$-D_{i,\text{mem}}\nabla C_{i,\text{mem}}^{'} = 0 \tag{6}$$

This equation in cylindrical coordinates is expressed by Eq. (7):

$$-D_{i,\text{mem}}\left[\frac{\partial^2 C_{i,\text{mem}}^{'}}{\partial R^2} + \frac{1}{R}\frac{\partial C_{i,\text{mem}}^{'}}{\partial R} + \frac{\partial^2 C_{i,\text{mem}}^{'}}{\partial Z^2}\right] = 0 \tag{7}$$

The solute transfer in the shell of the module occurs through diffusion and convection, and is described by following steady-state continuity equation:

$$D_{i,\text{org}}\left[\frac{\partial^2 C_{i,\text{org}}^{'}}{\partial R^2} + \frac{1}{R}\frac{\partial C_{i,\text{org}}^{'}}{\partial R} + \frac{\partial^2 C_{i,\text{org}}^{'}}{\partial Z^2}\right] = u_{z,\text{org}}\frac{\partial C_{i,\text{org}}^{'}}{\partial z} \tag{8}$$

where $C_{i,\text{org}}^{'}$ is the concentration of solute in the shell (flow-cell) of the module.

The velocity distribution in the shell side was calculated by using Navier–Stokes equation and was then coupled with continuity equation to characterize the flow in the shell side and to find the concentration profile of solute in this region. Navier–Stokes equation for incompressible flow under steady condition is given as [41]:

$$\rho u.\nabla u - \nabla.\mu(\nabla u + (\nabla u)^T + \nabla p = F, \qquad \nabla u = 0 \tag{9}$$

where ρ denotes density, *u* the velocity vector, μ the dynamic viscosity, *p* the pressure and *F* the body force term such as gravity. Gravity forces are ignored as the module was installed horizontally during experimentation. The boundary conditions for these equations are summarized in Table 2.

3.3. Numerical simulations

Model equations summarized above were solved using CFD techniques in COMSOL Multiphysics™ software. COMSOL software uses numerical finite element method (FEM) to solve mathematical equations. The finite element analysis was combined with adaptive meshing and error control using numerical solver of UMFPACK. This solver was well suited for solving stiff and non-stiff, non-linear boundary value problems [42]. A scale factor of 200 was applied in axial direction due to the large difference between length and radius of the module. "Scaling" avoided the excessive number of meshes and nodes thus minimized the calculation time. Adaptive mesh refinement was used to generate small meshes across the membrane and near the mass transfer boundaries. This was important near the interfaces especially where the fluid dynamics was the most sensitive to the conditions and the most influential on the overall mass transfer [43]. The COMSOL mesh generator thus generated around 13,000 triangular elements of varying sizes. Geometrical and simulation parameters of HFMC module are provided in Table 1. The numerical scheme adopted for solving the equations is shown in Fig. 3. Axial–radial magnified mesh of module geometry is shown in Fig. 4. The numerical and dynamic models were coupled and integrated in Matlab.

Table 2
Boundary conditions of copper (II) transport in HFMC

Boundary	Fiber side	Membrane	Shell side	Momentum transport
$z = 0$	$C_{in} = C_0$	Symmetry	Convective flux	–
$r = 0$	Axial symmetry	–	–	–
$r = R_1$	$C_1 = C_2/P$	$C_2 = P * C_1$	–	–
$r = R_2$	–	$C_2 = C_3$	$C_3 = C_2$	Wall, no slip condition
$r = R_3$	–	–	$\partial C_3/\partial r = 0$ (symmetry)	Wall, no slip condition (when R_3 shows shell of module) Axial symmetry (when R_3 shows shell of assumed flow-cell)
$z = L$	Convective flux	Symmetry	$C_{in} = 0$	$u = u_{in}$

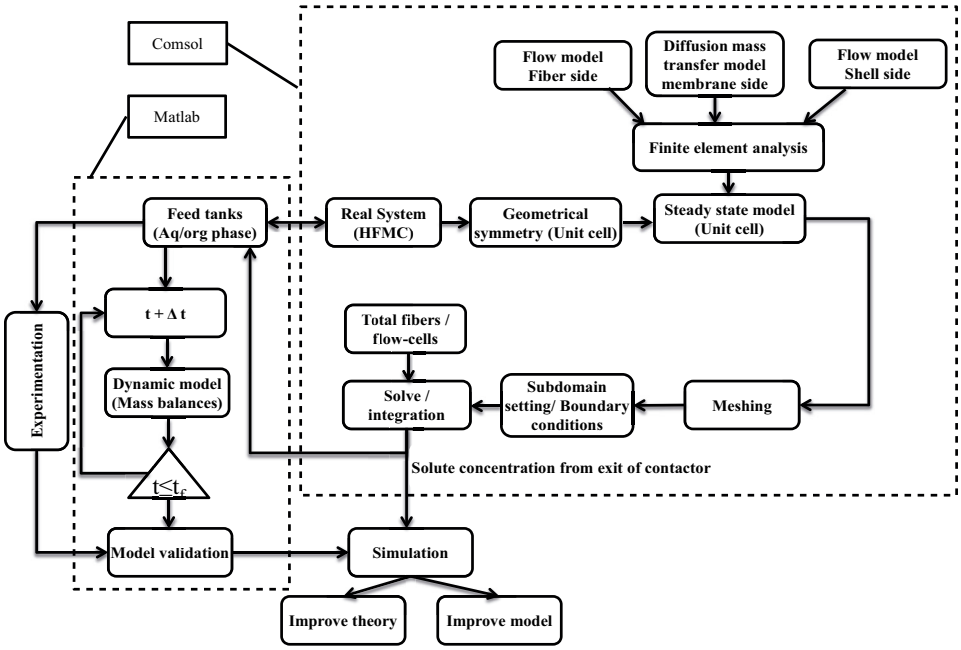

Fig. 3. Model algorithm/numerical scheme.

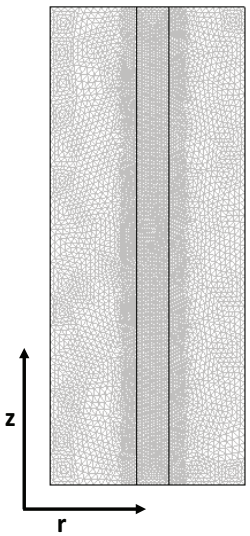

Fig. 4. Axial–radial magnified mesh screens of the flow-cell.

4. Results and discussion

4.1. Model validation

4.1.1. Steady-state once-through mode

The developed model was validated for both once-through (steady state) and recycled (dynamic) modes. For once through, the aqueous solution and spent solvent were not recycled and collected in different tanks after passing through the contactor. Concentration of copper (II) was measured at the outlet of contactor for different partition coefficients. Initial copper (II) concentration in aqueous feed was taken as 3.15 mol.m^{-3}, while initial concentration of TFA in 1-decanol was varied from 83 to 1,230 mol.m^{-3} in order to achieve the required partition coefficients. These values are listed in Table 3. Experiments were performed at 298 K, and pH was maintained at 4.96 (±0.2). These parameters were continuously monitored and controlled as they could alter the partition coefficient [16]. Experiments were run to investigate the extraction of solute at these four selected partition coefficients. Results obtained from experimental setup were

Table 3
Comparison of simulation results with experimental data for different partition coefficients: C_{ini} = 3.15 mol.m^{-3}, pH = 4.96, T = 298 K

Initial concentration of TFA, mol.m^{-3}	P	$C_{z=L}/C_0$ (Sim)	$C_{z=L}/C_0$ (Exp)	% Std. Deviation
83	0.5	0.81	0.98	8.73
160	1.0	0.70	0.79	5.66
855	4.1	0.38	0.41	3.47
1,230	6.9	0.13	0.12	2.43

compared with those of simulation as given in Table 3. It can be observed that good agreement exists between experimental data and model findings for higher partition coefficient. Model results deviated for lower value of partition coefficient. While performing the simulation, it was assumed that partition coefficient remained constant; however, the partition coefficient changes as the feed and solvent move along contactor. A higher partition coefficient means greater affinity of solvent for solute. Solubility of solute slightly changes when a higher partition coefficient is used. However, in case of lower partition coefficient, the effect on solubility is significant.

4.1.2. Unsteady-state recycled mode

In order to validate the model for recycled mode, simulations were compared with extraction experiments of copper (II) from aqueous solutions using the organic extractant phase (n-decanol) containing TFA (described in section 2). Unsteady-state mass balance was carried out around the feed and extractant considering an extended model in total recycled mode and to obtain the copper (II) concentration in feed tank. The developed dynamic model around the feed tank was given as follows [16]:

$$C_t\left(t+\Delta t\right)=\frac{\Delta t}{T_{aq}}C_{z=L}\left(t\right)+C_t\left(t\right)\left[1-\frac{\Delta t}{T_{aq}}\right] \tag{10}$$

where T_{aq} is the mean residence time, given by Eq. (11):

$$T_{aq}=\frac{V_{aq}}{Q_{aq}} \tag{11}$$

where V_{aq} was the volume of feed tank, and Q_{aq} was the volumetric flow rate. $C_t(t)$ and $C_t(t+\Delta t)$ were the concentration of copper (II) in the tank or at inlet of the contactor at time t and $t+\Delta t$, respectively. $C_{z=L}(t)$ was the copper (II) concentration at the exit of the contactor entering back into the feed tank at time t. This concentration was calculated using following equation:

$$C_{z=L}=\frac{\int C\left(r\right)ds}{\int ds} \tag{12}$$

where S is the area of tube side.

Similar equation could also be developed for copper (II) concentration in the organic phase tank.

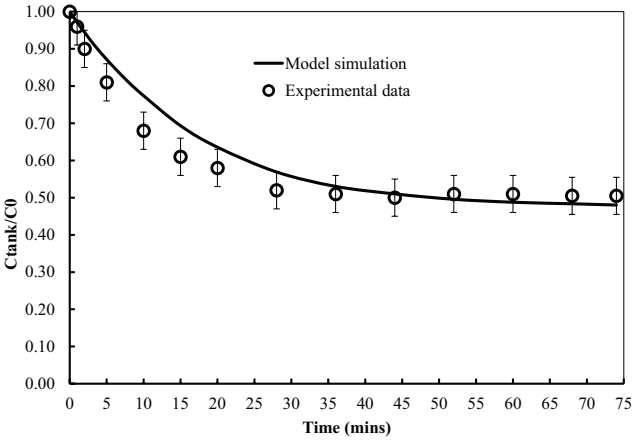

Fig. 5. Comparison of model results with experimental data: C_{in} (Cu^{2+}) = 3.15 mol.m^{-3}, C_{in} (TFA) = 160 mol.m^{-3}, P = 1, v_{aq} = 0.0033 m.s^{-1}, v_{org} = 0.0017 m.s^{-1}, and T = 298 K.

The algebraic model Eq. (10) was coupled with the numerical model (Eqs. (1)–(9)) and solved in Matlab. Simulation was carried out according to the scheme presented in Fig. 3. The results were compared with experimental data of copper (II) concentration in feed tank. The operational and structural parameters used in model simulation were the same as for experimental data. The results were plotted as copper (II) concentration to initial concentration in feed tank as a function of time in Fig. 5. The figure shows a good agreement between model predictions and experimental data. A slight deviation may be observed in the first 30 min; however, this behavior could be done by the low value of partition coefficient equal or less than 1 as the case is in current simulation where partition coefficient value of 1 has been taken. If a higher partition coefficient was used, the model would be more accurate (as shown for steady state). The same trends have been observed in a previous study published by Younas et al. [16], where model results matched very well with experimental data for the highest values of partition coefficient. It can also be noted from Fig. 5 that the concentration drop is rapid at the start of the extraction process in early 20 min of continuous recycling. This is due to higher concentration gradient in early extraction. However, as far as the extraction process progress, the concentration gradient across the membrane pores decreases, and thus, the rate of transfer of copper (II) decreases.

4.2. Profiles study

4.2.1. Velocity profile

The velocity plays an important role in the design and performance of HFMCs for liquid–liquid extraction. Simulation was carried out to observe the velocity distribution of organic phase in the "flow-cell" (shell) of HFMC based on parameters reported in Table 1. Axial–radial velocity profiles in the shell of module are plotted in Fig. 6. There are two types of velocity profiles in the annulus of imaginary flow-cell. For the flow-cells near the shell of module velocity as given in Fig. 6(a), here R_3 is a solid boundary (shell of module), and

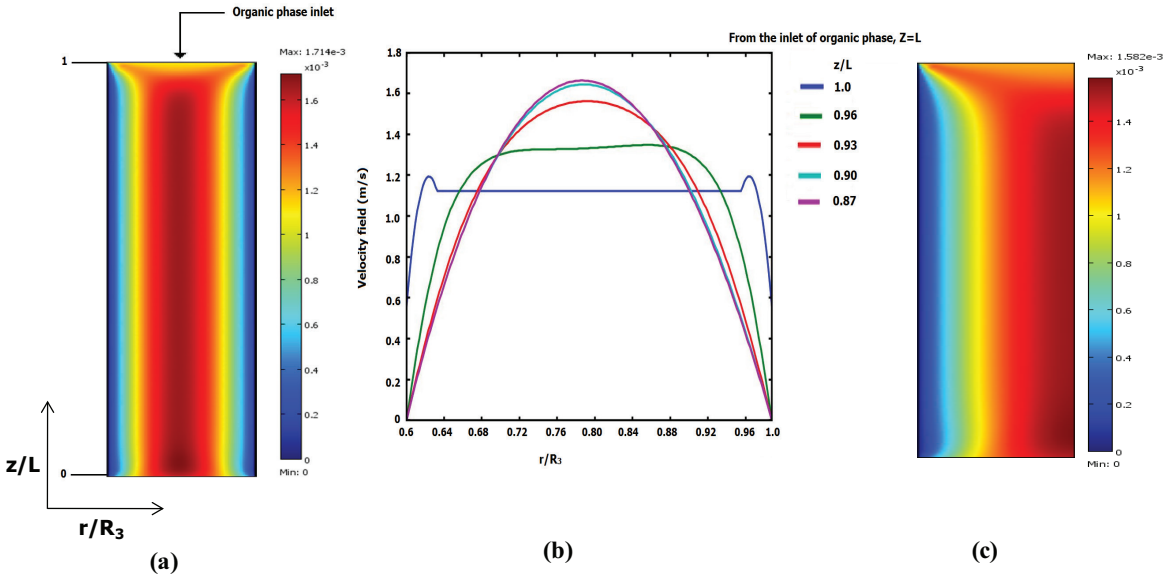

Fig. 6. Velocity profile in shell: (a) 2-D field distribution where R_3 shows shell of module, (b) radial profile and (c) 2-D field distribution where R_3 shows symmetry boundary: C_{in} (Cu^{2+}) = 3.15 mol.m^{-3}, C_{in} (TFA) = 160 mol.m^{-3}, P = 1, v_{aq} = 0.0033 m.s^{-1}, v_{org} = 0.0017 m.s^{-1}, and T = 298 K.

hence, no slip condition is assumed. It can be clearly observed that flow is in developing stage near the inlet of the module, i.e., velocity profile is not parabolic in this region. This velocity field is drawn in Fig. 6(b) for velocity of organic phase in "flow-cell" vs. radius at different positions of module length. Velocity variation can be seen from entrance till z/L = 0.87. At this point, the flow becomes fully developed. The maximum velocity of 0.0017 m.s^{-1} is noted in the center of the "flow-cell"; the corresponding Reynolds number is equal to 0.05. Fig. 6(c) shows velocity profile inside module where a symmetry has been assumed at $r = R_3$, and hence, a maximum velocity can be observed at this imaginary boundary.

The flow characterization in "flow-cell" is described by means of the Navier–Stokes equation. The entry effects are also taken into account using this approach, which increases the accuracy of the model.

4.2.2. Flux distribution profile

Fig. 7 shows the copper (II) flux distribution inside the fiber along the length of the module. The transport of copper (II) takes place due to convection and diffusion. Copper (II) is transferred from aqueous phase across the porous membrane in r-direction because of the concentration gradient. The mass transfer in radial direction is governed by molecular diffusion [44]. Simulations were performed with a partition coefficient value equal to 1.0, which is coherent with the assumption of instantaneous transfer of copper (II) by total complexation at the aqueous-organic interface. The Reynolds number of aqueous and organic phases in the fiber and "flow-cell" were equal to 0.73 and 0.05, respectively. It can be observed that convective flux in z-direction (axial) is predominant upon axial diffusive flux. This is due to the fact that velocity is significant in axial direction, which causes high convective flux of copper (II). A maximum convective flux is observed

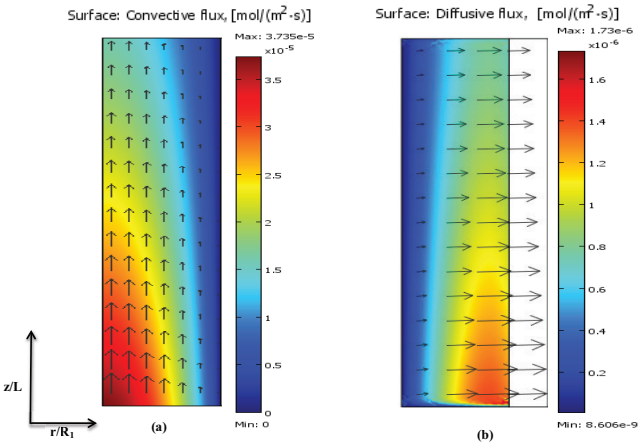

Fig. 7. (a) Axial–radial convective flux field in fiber side and (b) axial–radial diffusive flux field in fiber side. Feed concentration C_{in} (Cu^{2+}) = 3.15 mol.m^{-3}, C_{in} (TFA) = 160 mol.m^{-3}, P = 1, v_{aq} = 0.0033 m.s^{-1}, v_{org} = 0.0017 m.s^{-1}, and T = 298 K.

near the center of the fiber, as the velocity in this region is the highest one. Thus, diffusion is dominant in radial direction or in the boundary layers adjacent to porous membrane. Convection is dominant in axial direction, and velocity of aqueous phase affects the transport of copper (II) along the axis of module length. However, to increase the removal rate of copper (II) from aqueous phase, concentration gradient in r-direction should be enhanced. This can be achieved by using aqueous and organic phases with higher diffusivities of copper (II). Diffusion coefficient may be increased with increasing temperature; however, a higher temperature may degrade membrane material, so the factor must be kept in mind while selecting the process temperature.

It can also be observed from Fig. 7 that diffusive flux is higher in *r*-direction at the feed inlet. For example, at $z/L = 0.2$, diffusive flux increases from 0 to 1.2×10^{-6} mol $m^{-2}.s^{-1}$ in *r*-direction from $r = 0$ to $r = R_1$, i.e., from the center of tube toward the membrane pores entrance. At $z/L = 0.8$, the flux is enhanced from 0 to 8.3×10^{-7} mol $m^{-2}.s^{-1}$, which represents 69% of the earlier one. Copper (II) concentration is higher at $z/L = 0.2$ as compared with that at $z/L = 0.8$. More copper (II) is available for transport at earlier point, which consequently increases the flux of copper (II) and vice versa at later point. As a result, copper (II) concentration falls, and thus, *r*-direction flux is reduced as the feed moves along the *z*-axis of the module.

Diffusive and convective flux is calculated radially inside the fiber in the middle of the module at $z/L = 0.5$. The flux is plotted vs. r/R_1 in Fig. 8. $r/R_1 = 0$ indicates the center of fiber while $r/R_1 = 1$ shows the boundary of fiber wall. It can be observed that convective flux is maximum at the center of the fiber and is calculated to be 2.53×10^{-5} mol.$m^{-2}.s^{-1}$ while diffusive flux is found to be 0.42×10^{-7} mol.$m^{-2}.s^{-1}$ at that point. Diffusive flux then increases while convective flux decreases in radial direction. Diffusive flux becomes maximum in the boundary layer of aqueous phase achieving 10.44×10^{-7} mol.$m^{-2}.s^{-1}$. It can be inferred that convection is dominant in the center of the fiber. Nevertheless, copper (II) transport in boundary layer near the fiber wall is dominated by diffusion. Increasing the diffusion will increase the removal efficiency of solute. This can be achieved by lowering the velocity or by using an effective extractant with higher partition coefficient [16,40].

4.2.3. Concentration profile of copper (II)

Assembly of single fiber and "flow-cell" as sketched in Fig. 1 was simulated in 2-D and 3-D. The concentration of copper (II) was calculated radially in direction of flow along the length of module. Dimensionless concentration profile C/C_0 of copper (II) is plotted in Fig. 9 in 2-D for countercurrent flow, in all three compartments in which the transport of copper (II) is involved, i.e., inside the fiber, the membrane pores and the shell side. Feed enters at $z = 0$ inside fibers with copper (II) initial concentration of 3.15 mol m^{-3}. Organic phase flows countercurrently in shell of the module at $z = L$ with TFA (II) initial concentration of 160 mol.m^{-3}. Fig. 9 indicates that organic phase fills the pores of membrane and immobilizes in the fiber at membrane mouth. The reaction of copper (II) with TFA is considered instantaneous and is simply considered through the partition coefficient at the interface between the aqueous phase boundary layer to that of the organic phase at the membrane's mouth. The TFA-copper complex molecule diffuses through the membrane pores into shell side due to concentration gradient and is then swept out by the incoming organic phase.

Concentration profile plotted in Fig. 9 indicates the decrease of copper (II) concentration in the aqueous phase flows along the module length in *z*-axis. On the other hand, the concentration of TFA-copper complex in organic phase increases along its flow path. This behavior is given by the continuous transfer of copper (II) from aqueous feed to organic phase. It can also be observed that the decrease in copper (II) concentration in aqueous phase is smooth through the module length under the stated hydrodynamics conditions. Copper concentration falls to half of its initial value at exit, i.e., at $z/L = 1$ for once through under given conditions. However, this is not always the case. The fall in concentration strongly depends upon the partition coefficient. Changing the partition coefficient alters the concentration profile. For a partition coefficient greater than unity, the fall in copper (II) concentration is higher near the inlet and then decreases slowly throughout the module. A higher partition coefficient means greater affinity of TFA toward copper (II).

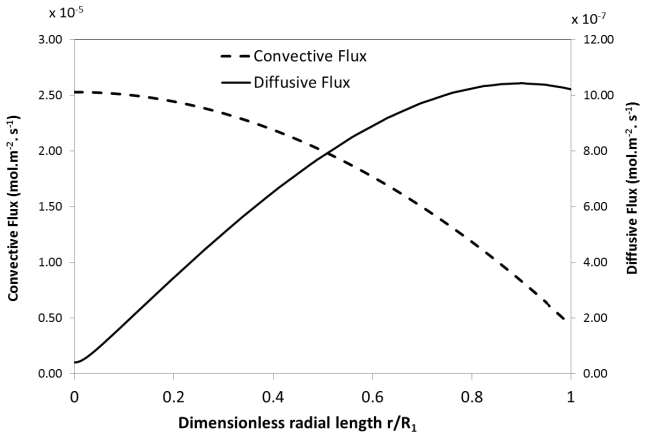

Fig. 8. Radial profiles of convective and diffusive flux at $z/L = 0.5$. Feed concentration $C_{in}(Cu^{2+}) = 3.15$ mol.m^{-3}, C_{in} (TFA) = 160 mol.m^{-3}, $P = 1$, $v_{aq} = 0.0033$ m.s^{-1}, $v_{org} = 0.0017$ m.s^{-1}, and $T = 298$ K.

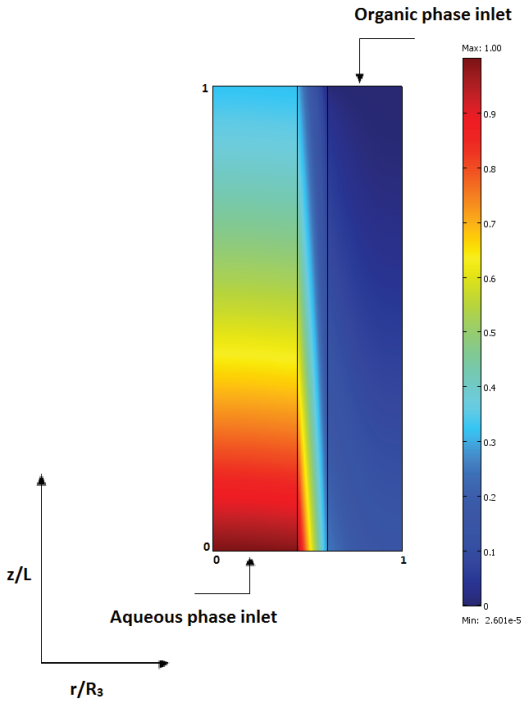

Fig. 9. 2-D concentration profile of a "flow-cell", C_all/C_0. Feed concentration C_{in} (Cu^{2+}) = 3.15 mol.m^{-3}, C_{in} (TFA) = 160 mol.m^{-3}, $P = 1$, $v_{aq} = 0.0033$ m.s^{-1}, $v_{org} = 0.0017$ m.s^{-1}, and $T = 298$ K.

4.3. Effects of process parameters on extraction efficiency

4.3.1. Effect of partition coefficient

Partition coefficient is an important parameter in liquid–liquid extraction process. It is defined as the ratio of solute concentration in organic phase to that of aqueous phase at equilibrium. To study the effects of partition coefficient using the current mathematical model, simulations were performed for arbitrarily selected values of partition coefficient. Flow rates of aqueous and organic phases were kept constant at 8.3×10^{-7} and 1.0×10^{-6} $m^3.s^{-1}$, respectively. It can be observed that an increase in partition coefficient increases the extraction of copper (II) across the membrane. Extraction efficiency is measured by taking the percentage ratio of copper (II) transferred from aqueous to organic phase to total copper (II) concentration available at module inlet in aqueous phase. Extraction efficiency of copper (II) removal from aqueous phase in once-through mode has been measured and plotted as function of partition coefficient in Fig. 10. Efficiency was calculated as follows:

$$\text{Efficiency} = \left(1 - \frac{C_{z=L}}{C_0}\right) \times 100 \quad (13)$$

It was found that the extraction efficiency increases much more rapidly at low values of partition coefficient. On the other hand, at higher values, the partition coefficient has a very little effect on extraction efficiency. For example, extraction efficiency of copper (II) transport is 34% with a partition coefficient equal to 2. Extraction efficiency increases at the rate of 23% per unit value till partition coefficient value of 4. Above this value, extraction efficiency increases exponentially and become negligible at values greater than 8. This means that there is no need to find an extractant or diluent with which the solute achieves a very high partition coefficient (that may either be toxic or expensive). Nevertheless, too small partition coefficient, i.e., a value near the unity, will result in low extraction efficiency. Nevertheless, it should be kept in mind that partition coefficient is not the only parameter that affects the extraction efficiency; feed flow rate has also a great effect on removal of solute. These effects are explained in the subsequent section. However, the same trends for partition coefficient effects on extraction can be observed for any value of flow rate used. Partition coefficient depends on various factors like the nature of extractant, pH, temperature and type of diluents [16,45].

4.3.2. Effects of flow rates

Interest has also been taken to investigate the effects of flow rates on extraction efficiency. Simulation was performed to measure the extraction efficiency of copper (II) from aqueous phase at partition coefficient equals to one. Copper (II) concentration was calculated at the inlet and outlet of HFMC module at various flow rates. Extraction efficiency was calculated for different values of flow rates of aqueous and organic phases. Flow rate of one phase was varied at a time while that of other phase was kept constant, and the result has been plotted in Fig. 11. It is indicated from the Fig. 11 that the extraction efficiency decreases with increasing aqueous phase (feed) flow rate. This is due to the fact that the contact or residence time of copper (II) decreases as the flow rate increases, resulting in lower mass transfer across the membrane. However, the increase in organic flow rate in shell side has the opposite effect on extraction efficiency of copper (II). The extraction efficiency increases with increasing organic flow rate as shown in Fig. 11. In fact increase in organic phase flow rate provides more TFA (extractant) to be in contact with copper (II) in the pores of the membrane. Thus, more copper (II) molecules are extracted from aqueous phase to organic phase. Increasing the flow rate of organic phase in shell side decreases the concentration of copper (II) at the membrane-shell interface and thus results in higher concentration gradient, which in turn increases the mass transfer [27]. It can also be observed that this effect is significant only at low flow rates. The effect on extraction efficiency becomes negligible at flow rate of organic phase greater than 8.0×10^{-8} $m^3.s^{-1}$. Because no more solute is available for removal at boundary layer of organic phase in shell side at higher flow rate. Nevertheless, Marjani and Shirazian [44] reported that organic flow rate has negligible effects on extraction

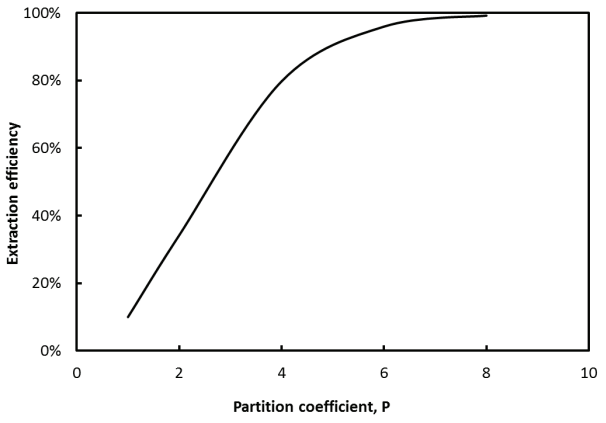

Fig. 10. Effect of partition coefficient on extraction efficiency. Feed concentration C_{in} (Cu^{2+}) = 3.15 $mol.m^{-3}$, C_{in} (TFA) = 160 $mol.m^{-3}$, v_{aq} = 0.0033 $m.s^{-1}$, v_{org} = 0.0017 $m.s^{-1}$, and T = 298 K.

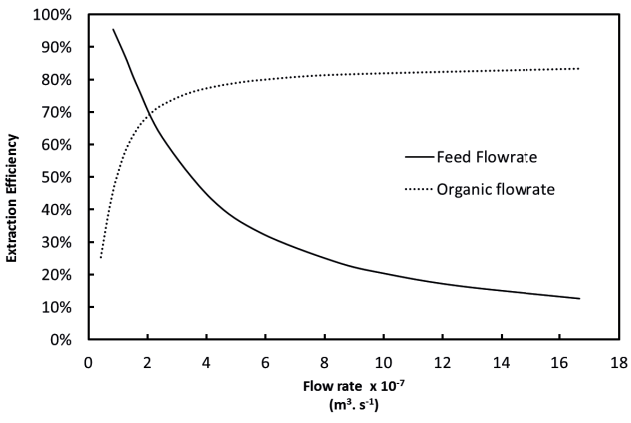

Fig. 11. Effects of aqueous and organic flowrates on extraction efficiency. C_{in}(Cu) = 3.15 $mol.m^{-3}$, C_{in}(TFA) = 160 $mol.m^{-3}$, P = 1, T = 298 K.

efficiency. However, it is true for only high flow rate values of organic phase. Meanwhile, these effects are significant at lower flow rate values. Fadaei et al. [35] have also showed increase in extraction efficiency of solute with the increase of organic phase flow rate. However, this increase was not significant. They found that extraction efficiency ranges from 12% to 65% when feed flow rate is varied from 1×10^{-8} to 9×10^{-8} $m^3.s^{-1}$ for a constant organic flow rate of 1×10^{-8} $m^3.s^{-1}$. In current study, copper (II) extraction efficiency was found to reach 95% while flow rate was ten times greater as reported in previous studies.

5. Conclusions

A numerical model was developed for extraction of copper (II) with TFA diluted in n-decanol using HFMC. Fibers were considered as straightened and parallel to each other. A hypothetical "flow-cell" was assumed surrounding each fiber. CFD simulation was performed using coupling of mass and momentum transport equations. Numerical CFD model was then integrated with dynamic model developed across the feed tank. The integrated model was successfully validated with experimental results for the extraction of copper (II) with TFA. Extraction efficiency of 49% has been determined in about 60 min of recycled-based extraction of copper (II) for partition coefficient equal to 1. Extraction efficiency greatly depends upon partition coefficient and feed flow rate. It increases exponentially with partition coefficient and decreases with feed flow. Steady-state CFD simulation of HFMC revealed that diffusion and convection controlled regions along the path of feed flow strongly depend on the feed flow rate and partition coefficient. The 2-D simulation permits the visualization of concentration, velocity and flux distribution both axially and radially.

Symbols

C — Concentration, $mol.m^{-3}$
C' — Dimensionless concentration
D — Diffusion coefficient, $m^2.s^{-1}$
F — Body force term (N) such as gravity, N
N — Combined flux (diffusive + convective), $mol.m^{-2}.s^{-1}$
n — Number of fibers
P — Partition coefficient
p — Pressure, $N.m^{-2}$
P_f — Packing fraction
Q — Volumetric flow rate, $m^3.s^{-1}$
Re — Reynolds number
R' — Rate of reaction, s^{-1}
R — Radius, m
r — Radial axis, m
u — Mean velocity, $m.s^{-1}$
V — Volume of tank, m^3
v — Velocity, $m.s^{-1}$
T — Time constant, min
t — Time, min
ρ — Density, $kg.m^{-3}$
μ — Dynamic viscosity, pa.s
ε — Porosity
τ — Tortuosity
∇ — Gradient vector

Subscripts

1 — Fiber side boundary layer
2 — Membrane pores
3 — Shell side boundary layer
aq — Aqueous phase
i — Specie, solute (copper (II))
in — Inlet
mem — Membrane
org — Organic phase
r — Radial axis
z — Axial axis

References

[1] C. Yun, R. Prasad, K.K. Sirkar, Hollow fiber solvent extraction removal of toxic heavy metals from aqueous waste streams, Ind. Eng. Chem. Res., 32 (1993) 1186–1194.
[2] M. Yang, E. Cussler, Reaction dependent extraction of copper and nickel using hollow fibers, J. Membr. Sci., 166 (2000) 229–238.
[3] R.S. Juang, H.L. Huang, Modeling of nondispersive extraction of binary Zn(II) and Cu(II) with D2EHPA in hollow fiber devices, J. Membr. Sci., 208 (2002) 31–38.
[4] M.J. Gonzalez-Mufioz, S. Luque, J.R. Alvarez, J. Coca, Simulation of integrated extraction and stripping processes using membrane contactors, Desalination, 163 (2004) 1–12.
[5] A. Kiani, R.R. Bhave, K.K. Sirkar, Solvent extraction with immobilized interfaces in a microporous hydrophobic membrane, J. Membr. Sci., 20 (1984) 125–145.
[6] S.B. Iversen, V.K. Bhatia, K. Dam-Johansen, G. Jonsson, Characterisation of microporous membranes for use in membrane contactors, J. Membr. Sci., 130 (1997) 205–217.
[7] A.K. Pabby, A.M. Sastre, Hollow Fiber Membrane-Based Separation Technology: Performance and Design Perspectives, M. Aguilar, J.L. Cortina, Eds., Solvent Extraction and Liquid Membranes, Taylor & Francis Group, LLC, New York, 2008, pp. 91–140.
[8] R. Prasad, K.K. Sirkar, Membrane-Based Solvent Extraction, W.S.W. Ho, K.K. Sirkar, Eds., Membrane Handbook, Chapman & Hall, New York, 1992, pp. 727–763.
[9] M.C. Yang, E.L. Cussler, Designing hollow fiber contactors, AIChE J., 32 (1986) 1910–1915.
[10] A. Gabelman, S.T. Hwang, Hollow fiber membrane contactors, J. Membr. Sci., 159 (1999) 61–106.
[11] A.K. Pabby, A.M. Sastre, State-of-the-art review on hollow fiber contactor technology and membrane-based extraction processes, J. Membr. Sci., 430 (2013) 263–303.
[12] E. Bringas, S.M.F. Rom, J.A. Rabien, I. Ortiz, An overview of the mathematical modeling of liquid membrane separation processes in hollow fibre contactors, J. Chem. Technol. Biotechnol., 84 (2009) 1583–1614.
[13] S.B. Hu, J.M. Wiencek, Emulsion-liquid membrane extraction of copper using a hollow fiber contactor, AIChE J., 44 (1998) 570–58.
[14] A.M. Urtiaga, M.J. Abellan, J.A. Irabien, I. Ortiz, Membrane contactors for the recovery of metallic compounds: modelling of copper recovery from WPO processes, J. Membr. Sci., 257 (2005) 161–170.
[15] B. Sengupta, M.S. Bhakhar, R. Sengupta, Extraction of copper from ammoniacal solutions into emulsion liquid membranes using LIX 84-I, Hydrometallurgy, 89 (2007) 311–318.
[16] M. Younas, S.D. Bocquet, J. Sanchez, Experimental and theoretical mass transfer transient analysis of copper extraction using HFMCs, J. Membr. Sci., 82 (2011) 70–81.
[17] M. Younas, S.D. Bocquet, J. Romero, J. Sanchez, Experimental and theoretical investigation of distribution equilibria and kinetics of copper (II) extraction with LIX 84-I and TFA, Sep. Sci. Technol., 50 (2015) 1523–1531.
[18] R.S. Juang, H.L. Huang, Mechanistic analysis of solvent extraction of heavy metals in membrane contactors, J. Membr. Sci., 213 (2003) 125–135.

[19] S.D. Bocquet, A. Torres, J. Sanchez, G.M. Rios, J. Romero, Modeling the mass transfer in solvent extraction processes with hollow-fiber membranes, AIChE J., 51 (2005) 1067–1079.
[20] R. Ghidossi, D. Veyret, P. Moulin, Computational fluid dynamics applied to membranes: state of the art and opportunities, Chem. Eng. Process., 45 (2006) 437–454.
[21] R. Kieffer, C. Charcosset, F. Puel, D. Mangin, Numerical simulation of mass transfer in a liquid-liquid membrane contactor for laminar flow conditions, Comput. Chem. Eng., 32 (2008) 1325–1333.
[22] A. Cipollina, G. Micale, I. Rizzuti, Membrane distillation heat transfer enhancement by CFD analysis of internal module geometry, Desal. Wat. Treat., 5 (2011) 195–209.
[23] J. Oh, D. Jeong, I. Yum, Y. Lee, A numerical analysis for CO_2 recovery from aqueous absorbent solution by hollow fiber membrane contactor, Desal. Wat. Treat., 17 (2010) 218–226.
[24] R. Faiz, M. Al-Marzouqi, CO_2 removal from natural gas at high pressure using membrane contactors: model validation and membrane parametric studies, J. Membr. Sci., 365 (2010) 232–241.
[25] M.R. Sohrabi, A. Marjani, S. Shirazian, S. Moradi, Acetone and ethanol extraction from water by means of membrane: modeling and numerical simulation, Middle East J. Sci. Res., 7 (2011) 530–537.
[26] S.M.R. Razavi, S.M.J. Razavi, T. Miri, S. Shirazian, CFD simulation of CO_2 capture from gas mixtures in nanoporous membranes by solution of 2-amino-2-methyl-1-propanol and piperazine, Int. J. Greenhouse Gas Control, 15 (2013) 142–149.
[27] M. Al-Marzouqi, M. El-Naas, S. Marzouk, N. Abdullatif, Modeling of chemical absorption of CO_2 in membrane contactors, Sep. Purif. Technol., 62 (2008) 499–506.
[28] M. Al-Marzouqi, M.H. El-Naas, S.A.M. Marzouk, M.A. Al-Zarooni, N. Abdullatif, R. Faiz, Modeling of CO_2 absorption in membrane contactors, Sep. Purif. Technol., 59 (2008) 286–293.
[29] M. Rezakazemi, Z. Niazi, M. Mirfendereski, S. Shirazian, T. Mohammadi, A. Pak, CFD simulation of natural gas sweetening in a gas–liquid hollow-fiber membrane contactor, Chem. Eng. J., 168 (2011) 1217–1226.
[30] M. Mahdavian, H. Atashi, M. Zivdar, M. Mousavi, Simulation of CO_2 and H_2S removal using methanol in hollow fiber membrane gas absorber (HFMGA), Adv. Chem. Eng. Sci., 2 (2012) 50–61.
[31] A. Marjani, S. Shirazian, Application of CFD techniques for prediction of NH_3 transport through porous membranes, Orient. J. Chem., 28 (2012) 67–72.
[32] M. Rezakazemi, S. Shirazian, S.N. Ashrafizadeh, Simulation of ammonia removal from industrial wastewater streams by means of a hollow-fiber membrane contactor, Desalination, 285 (2012) 383–392.
[33] N. Nosratinia, M. Ghadiri, H. Ghahremani, Mathematical modeling and numerical simulation of ammonia removal from wastewaters using membrane contactors, J. Ind. Eng. Chem., 20 (2014) 2958–2963.
[34] M. Ghadiri, S. Sherazian, Computational simulation of mass transfer in extraction of alkali metals, Chem. Eng. Process., 69 (2013) 57–62.
[35] F. Fadaei, S. Shirazian, S.N. Ashrafizadeh, Mass transfer simulation of solvent extraction in hollow-fiber membrane contactors, Desalination, 275 (2011) 126–132.
[36] R. Rigglo, H.E. Martinez, H.N. Solimo, Densities, viscosities, and refractive indexes for the methyl isobutyl ketone + pentanols systems. Measurements and correlations, J. Chem. Eng. Data, 31 (1986) 225–238.
[37] M.A.F. Faria, C.F. De-Sa, G.R. Lima, J.I.B.C. Filho, R.J. Martins, J.E.De-M. Car-doso, O.E. Barcia, Measurement of density and viscosity of binary 1-alkanol systems (C8–C11) at 101 kPa and temperatures from (283.15 to 313.5) K, J. Chem. Eng. Data, 50 (2005) 1938–1943.
[38] V. Mutalik, L.S. Manjeshwar, M. Sairam, T.M. Aminabhavi, Thermodynamic properties of (tetradecane + benzene, + toluene, + chlorobenzene, + bromobenzene, + anisol) binary mixtures at T = (298.15, 303.15, and 308.15) K, J. Chem. Thermodyn., 38 (2006) 1062–1071.
[39] C.B. Patil, P.K. Mohapatra, V.K. Manchanda, Transport of thorium from nitric acid solution by non-dispersive solvent extraction using a hollow fibre contactor, Desalination, 232 (2008) 272–279.
[40] M. Younas, S.D. Bocquet, J. Sanchez, Kinetic and dynamic study of liquid-liquid extraction of copper in a HFMC: experimentation, modeling, and simulation, AIChE J., 56 (2011) 1469–1480.
[41] R.B. Bird, W.E. Stewart, E.N. Lightfoot, Transport Phenomena, 2nd ed., John Wiley & Sons, New York, 1960.
[42] M. Fasihi, S. Shirazian, A. Marjani, M. Rezakazemi, Computational fluid dynamics simulation of transport phenomena in ceramic membranes for SO_2 separation, Math. Comput. Modell., 56 (2012) 278–286.
[43] M. Saeed, L. Deng, CFD Modeling of Hollow Fiber Membrane Contactor for Post-Combustion CO_2 Capture, 2nd Post Combustion Capture Conference (PCCC2), Bergen, Norway, 2013.
[44] A. Marjani, S. Shirazian, Simulation of heavy metal extraction in membrane contactors using computational fluid dynamics, Desalination, 281 (2011) 422–428.
[45] S.D. Bocquet, F.G. Viladomat, C.M. Nova, J. Sanchez, V. Athes, I. Souchon, Membrane-based solvent extraction of aroma compounds: choice of configurations of hollow fiber modules based on experiments and simulation, J. Membr. Sci., 281 (2006) 358–368.